A Novel Slot-PM Assisted Complementary-Rotor Doubly-Salient Machine with Enhanced Torque Performance

Sigao Wang, Xiaodong Zhang, Xing Zhao, Shuangxia Niu and W. N. Fu

Abstract—This paper presents a novel doubly salient permanent magnet (DSPM) machine with enhanced torque performance. The key is that an assistive magnetic flux is produced by using two sets of slot PMs inserted into the slot openings, which can effectively improve the torque production. Besides, a complementary magnetic path is built by dual rotors with 180° angle shift to reduce leakage flux, which can effectively suppress the torque ripple. In this paper, the proposed machine design is presented, including working principle, winding configuration, magnetic path analysis. Then, the Genetic Algorithm is used to find the optimal designs for the proposed machine. Further, to verify the effectiveness of the proposed machine, three doubly salient machines are compared, including the proposed machine, a DSPM machine without assistive slot PM design, and a dual-rotor DSPM machine without complementary rotor structure. Finally, a prototype of the proposed machine is built and tested to verify the validity of the proposed machine design.

Index Terms—Doubly salient, finite element analysis, permanent magnet machines, slot PM.

I. Introduction

WITH an increased transmission efficiency and reduced mechanical losses, direct-drive machines have been increasingly studied in recent years [1]. Among them, the doubly salient permanent magnet (DSPM) machine is a promising candidate thanks to its simple structure, low cost, high efficiency, and high reliability [2]-[4]. Unlike rotor-PM machines, the PMs of DSPM machines are assigned at the stator side, so that the PMs would not suffer from centrifugal force, and poor heat dissipation condition [5]-[7].

Traditional DSPM machines have PMs located at the stator yoke and there are three stator teeth between two adjacent PMs [8]. The static characteristics of this type of DSPM machine are investigated and a modeling method is investigated in [9], [10]. However, the torque density of this kind of DSPM machine is relatively low. To increase the torque production, in [11], a DSPM machine with 8/6-pole structure is proposed. The corresponding control strategies are developed in [12], [13]. However, it suffers from asymmetry machine structure and associated unbalanced coil flux which results in increased torque ripple. In [14], it is revealed that the torque production can be enhanced with symmetrical machine structures. Thus, to achieve symmetry structure, in [15], [16], "T-shaped" and "Π-shaped" stator core are investigated, in which only one or two stator teeth are assigned between adjacent PMs. Another solution to improve the torque density is to adopt stator slot-opening PMs in DSPM machines [17-21], in which the slot opening PMs are used together with DC windings or zero-sequence current in armature windings. The saturation of the stator core can be relieved with the slot opening PMs. However, the slot opening PMs are short-circuited in the magnetic path. Therefore, it cannot contribute to torque production directly. The torque density is raised but the PM ripple issue is still not addressed.

It is known that the relatively large torque ripple is mainly caused by unbalanced magnetic path and the leakage flux. [22] Although using "T-shaped" or "Π-shaped" stator core is a good approach to build symmetrical machine structures and balanced windings to suppress torque ripple, the torque ripple of the DSPM machine is still large because of the opened circuit magnetic path and associated leakage flux. It is desired to find a new design approach to effectively reduce the leakage flux so as to suppress the torque ripple in the DSPM machine.

However, there are few DSPM machine topologies which can give a thorough consideration in terms of torque promotion and ripple suppression. In this paper, a novel topology with two sets of auxiliary slot PMs and a complementary rotor structure is proposed. It is revealed in this paper that auxiliary PMs can contribute to an effective flux increment in armature winding, hence enhancing the torque production. Besides, the complementary rotor structure provides a magnetic flux complement in the magnetic path, hence avoiding open magnetic path and resultant flux leakage. And therefore, the torque ripple can be effectively suppressed.

In this paper, firstly, the machine structure and working principle are presented in Section II and III, respectively. In Section IV, the proposed machine is optimized with other DSPM machines by Genetic Algorithm within the same size and current density. Further, a comprehensive comparison among different models is presented to validate the effectiveness of the proposed topology. Finally, in Section V, a prototype is built and experimental validation is presented to verify the proposed design.

II. Machine Structure

A. Machine Topology and Winding Connecting Pattern

The structure of the proposed machine is shown in Fig. 1. All armature windings and PMs are assigned in the stator side and the rotors consist of iron core with salient poles only. The

cup-shaped dual rotors with the angular difference of 180º electrical degrees are connected to form a complementary magnetic path. One set of PMs is located at the yoke of the stator to build the main field, and two sets of PMs with the same magnetizing direction are located at the outer and inner slot openings to build the auxiliary field. There are two sets of armature windings connected in series housed in the inner and outer stator slots. The armature windings are connected in series with a double-layer concentrated configuration, as shown in Fig. 2. In this machine, there are 24 stator slots and 24 stator coils in the inner and outer stator slots. And each rotor has 22 teeth.
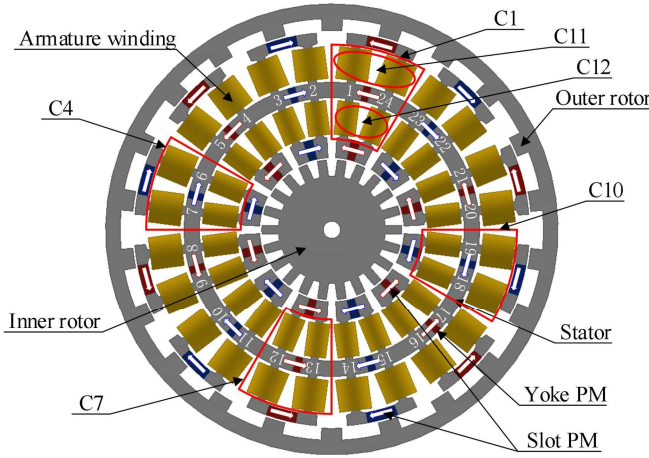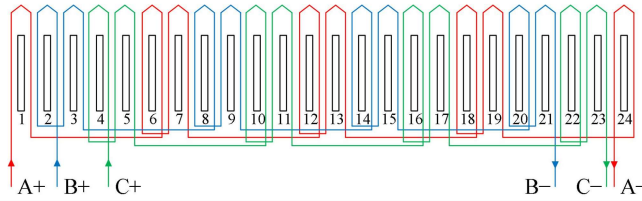

Fig. 1. Proposed machine structure.

Fig. 2. Armature winding configuration.

The features of the proposed machine are listed as follows.

(1) The slot opening PMs and yoke PMs are parallel-excited excitation sources. With the assistive slot PMs, an auxiliary magnetic flux is provided which is in phase with the main magnetic flux provided by the yoke PMs. Besides, the BH working range can be broadened and the stator core utilization factor can be improved. Hence, the torque is effectively enhanced.

(2) Complementary rotor structure is used to provide a commutative flux path for the magnetic field from PMs. Hence the opened magnetic path is avoided and the resultant leakage flux, as well as the cogging torque, are greatly suppressed. Since the DC components and even harmonics in excitation flux are reduced, the back-EMF harmonics are reduced and torque density is improved accordingly.

B. Main Flux and Auxiliary Flux Analysis

As shown in Fig. 1, Phase A winding is formed with four groups of coils, namely Coil $C1$, $C2$, $C7$, and $C10$. In Coil $C1$, $C11$ refers to the outer stator coil and $C12$ refers to the inner stator coil. The working principle of the proposed machine can

be explained with the open-circuit flux path distribution and the schematic flux fluctuation in coil $C1$ as shown in Fig. 3 and Fig. 4. $C11$ is composed of the two outer coils adjacent to yoke PM and $C12$ is composed of the two inner coils adjacent to yoke PM. The main magnetic flux Ψ_{C11_M} and Ψ_{C12_M} are built by the yoke PMs as shown in Fig. 3(a). The auxiliary field Ψ_{C11_I}, Ψ_{C12_I} are built by inner slot PMs and Ψ_{C11_O} and Ψ_{C12_O} are built by outer slot PMs as shown in Fig. 3(b). Here, the subscript M, I, and O refer to the main yoke PMs, inner slot PMs and outer slot PMs, respectively. When the rotor is at position A, namely outer rotor salient poles are aligned with stator teeth, the permeance in the outer rotor is higher, which provides a magnetic path for main magnetic flux to pass through the outer airgap. At this position A, the inner slot PMs provide an auxiliary magnetic flux Ψ_{C11_I} in outer stator coils $C11$ which are in phase with the main flux Ψ_{C11_M} from the yoke PMs as shown in Fig. 3(b). And considering the coil connection, the magnetic flux in the two coils are identical with each other, $\Psi_{C11\_I} = \Psi_{C12\_I}$. When the rotor is at position B where inner rotor salient poles are aligned with stator teeth, a complementary magnetic path passing through the inner air gap is provided. Similarly, $\Psi_{C12\_O} = \Psi_{C11\_O}$. Therefore, the outer slot PMs provide an auxiliary magnetic flux Ψ_{C12_O} which is in phase with the magnetic flux Ψ_{C12_M} from yoke PMs in the machine.
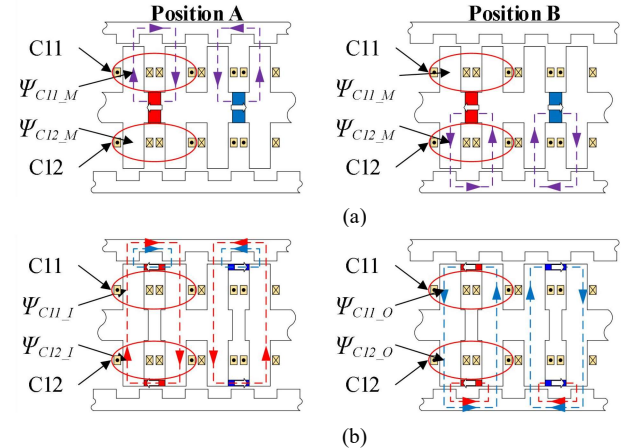

Fig. 3. Open-circuit magnetic flux distribution. (a) Main field from yoke PMs. (b) Auxiliary field from slot PMs.
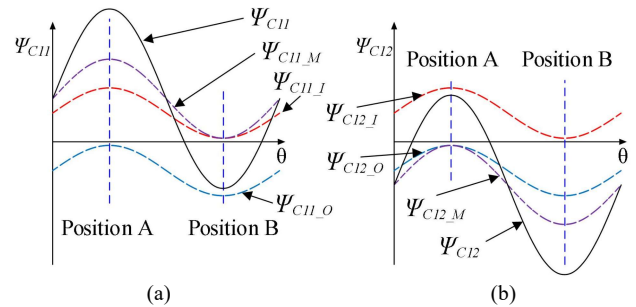

Fig. 4. Schematic open-circuit flux linkage at different rotor positions. (a) Magnetic flux in outer coils $C11$. (b) Magnetic flux in inner coils $C12$.

From Fig. 4, it is shown for coil $C11$, the auxiliary flux from inner and outer slot PMs (Ψ_{C11_I} and Ψ_{C11_O}) can effectively boost the positively biased main flux Ψ_{C11_M}. Similarly, for coil $C12$, the auxiliary flux from inner and outer slot PMs (Ψ_{C12_I} and Ψ_{C12_O}) can effectively boost the negatively biased main

flux Ψ_{C12_M}. Consequently, it is shown that the auxiliary magnetic flux from slot PMs is always in phase with the main magnetic flux, which consequently could effectively boost the torque production. Also, stator coils $C11$ and $C12$ can be connected in series to form coil $C1$.

III. MACHINE CHARACTERISTIC ANALYSIS

A. Single Coil Flux Analysis

To further explain the mechanism of the proposed DSPM machine with parallel-excited slot PMs and yoke PMs as well as the complementary flux path, the flux in the machine is analyzed in detail. As shown in Fig. 3, the main flux in the stator inner coils $C11$ and outer coils $C12$ produced from yoke PMs, denoted with Ψ_{C11_M} and Ψ_{C12_M}, can be expressed as

$$\psi_{C11\_M} = \psi_{DCC11\_M} + \sum_{n=1}^{+\infty} \psi_{ACC11\_Mn} cos(nN_r\theta) \tag{1}$$

$$\psi_{C12\_M} = -\psi_{DCC12\_M} - \sum_{n=1}^{+\infty} \psi_{ACC12\_Mn} cos\left[nN_r\left(\theta + \frac{\pi}{N_r}\right)\right] \tag{2}$$

where Ψ_{DCC11_M} and Ψ_{DCC12_M} are the corresponding biased DC components from yoke PMs, and subscript M refers to the main excitation source yoke PM. Ψ_{ACC11_Mn} and Ψ_{ACC12_Mn} are the amplitude of the nth order harmonic component. Subscript DC and AC refer to the DC component and AC harmonic components in the magnetic flux, respectively. When they are connected in series, the total flux (Ψ_{C1_M}) can be expressed as

$$\psi_{C1\_M} = \psi_{C11\_M} + \psi_{C12\_M}$$
$$= \psi_{DCC11\_M} - \psi_{DCC12\_M}$$
$$+ \sum_{n=1,3,5,...}\left(\psi_{ACC11\_Mn} + \psi_{ACC12\_Mn}\right)cos(nN_r\theta)$$
$$+ \sum_{n=2,3,6,...}\left(\psi_{ACC11\_Mn} - \psi_{ACC12\_Mn}\right)cos(nN_r\theta) \tag{3}$$

According to (3), the even-order harmonic components and DC component from coil $C11$ and coil $C12$ mitigate each other due to the complementary structure. If the two rotors and two sets of slot PMs are totally symmetrical in structure, the even-order harmonics and DC component would be canceled out. As shown in Fig.4, Ψ_{C11_M} is always positively biased and Ψ_{C12_M} is always negatively biased. Thus, with merely yoke PMs, the stator BH working range is limited within the first quadrant, providing biased magnetic flux in the stator teeth. To broaden the BH working range, two sets of slot PMs can be used. The auxiliary flux from inner and outer slot PMs in coil $C11$ and $C12$ can be expressed as:

$$\psi_{C11\_I} = \psi_{C12\_I} = \psi_{DCC11\_I} + \sum_{n=1}^{+\infty} \psi_{ACC11\_In} cos(nN_r\theta) \tag{4}$$

$$\psi_{C11\_O} = \psi_{C12\_O} = -\psi_{DCC11\_O} - \sum_{n=1}^{+\infty} \psi_{ACC11\_On} cos\left[nN_r\left(\theta + \frac{\pi}{N_r}\right)\right] \tag{5}$$

where Ψ_{C11_I}, Ψ_{C12_I}, Ψ_{C11_O}, and Ψ_{C12_O} are the flux from slot PMs in $C11$ and $C12$, and the subscript I and O refer to inner slot PMs and outer slot PMs, respectively. Ψ_{DCC11_I} is the DC component, and Ψ_{ACC11_In} is the amplitude of the nth harmonic component. When the two sets of slot PMs are used simultaneously, the total flux in two coils can be expressed as

$$\psi_{C11\_IO} = \psi_{C12\_IO} = \psi_{C11\_I} + \psi_{C11\_O}$$
$$= \psi_{DCC11\_I} - \psi_{DCC11\_O}$$
$$+ \sum_{n=1,3,5...}^{+\infty}\left(\psi_{ACC11\_In} + \psi_{ACC11\_On}\right)cos(nN_r\theta)$$
$$+ \sum_{n=2,4,6,...}^{+\infty}\left(\psi_{ACC11\_In} - \psi_{ACC11\_On}\right)cos(nN_r\theta) \tag{6}$$

where Ψ_{C11_IO} and Ψ_{C12_IO} are the flux from inner and outer slot PMs in $C11$ and $C12$, respectively. Similar to the main flux from yoke PMs, for the auxiliary flux from slot PMs, the odd components amplify each other, but the DC component and even harmonics from two groups of slot PMs mitigate each other. However, the BH working range is not limited to the first quadrant. And therefore the stator core can be better utilized when slot PMs are used.

When coil $C11$ and $C12$ are connected in series, the total flux (Ψ_{C1}) can be expressed as

$$\psi_{C1} = \psi_{C11} + \psi_{C12}$$
$$= \psi_{C11\_M} + \psi_{C11\_IO} + \psi_{C12\_M} + \psi_{C12\_IO} \tag{7}$$

By substituting (1), (2) and (6) into (7), we can further obtain the flux in coil $C1$

$$\psi_{C1} = \psi_{DCC11\_M} - \psi_{DCC12\_M} + 2\psi_{DCC11\_I} - 2\psi_{DCC11\_O}$$
$$+ \sum_{n=1,3,5,...}\left(\psi_{ACC11\_Mn} + \psi_{ACC12\_Mn} + 2\psi_{ACC11\_In} + 2\psi_{ACC11\_On}\right)cos(nN_r\theta)$$
$$+ \sum_{n=2,4,6,...}\left(\psi_{ACC11\_Mn} - \psi_{ACC12\_Mn} + 2\psi_{ACC11\_In} - 2\psi_{ACC11\_On}\right)cos(nN_r\theta)$$
$$= \psi_{DCC1} + \sum_{n=1,3,5...}\psi_{ACC1\_n} cos(nN_r\theta) + \sum_{n=2,4,6...}\psi_{ACC1\_n} cos(nN_r\theta) \tag{8}$$

Comparing (3) and (8), by using the slot PMs, the DC component and even harmonics are almost unchanged because the additional terms in DC component and even harmonics ($2\Psi_{DCC11\_I} - 2\Psi_{DCC11\_O}$ and $2\Psi_{ACC11\_In} - 2\Psi_{ACC11\_On}$) can be designed to be close to 0. However, for the odd harmonics, the amplitudes are greatly improved with the additional term ($2\Psi_{ACC11\_In} + 2\Psi_{ACC11\_On}$) from slot PMs. It implies that the DC component and even harmonics are suppressed in the excitation flux, but odd harmonics are greatly amplified with the slot PMs.

B. Complement Characteristic in Coils Belonging to the Same Phase

The flux in the other coils can be expressed as follows.

$$\psi_{Ck} = (-1)^{k+1}\left\{\psi_{DCCk}\right.$$
$$+ \sum_{n=1,3,5...} \psi_{ACCk\_n} cos\left[nN_r\left(\theta + \frac{4\pi(k-1)}{N_{slot}}\right)\right]$$
$$+ \left.\sum_{n=2,4,6...} \psi_{ACCk\_n} cos\left[nN_r\left(\theta + \frac{4\pi(k-1)}{N_{slot}}\right)\right]\right\} \tag{9}$$

where Ψ_{Ck} is the flux in coil Ck, it has the same amplitudes of DC and AC components as coil $C1$. The coil Ck should be connected with coil $C1$ to form the same phase if their fundamental harmonics are in phase with each other. Thus, (9) can be further expressed as

$$\psi_{Cm} = \psi_{DCCm} + \sum_{n=1,3,5...}\psi_{ACCm\_n} cos(nN_r\theta) + \sum_{n=2,4,6...}\psi_{ACCm\_n} cos(nN_r\theta),$$
$$m = odd\ number.$$

$$\psi_{Cm} = -\psi_{DCCm} + \sum_{n=1,3,5...}\psi_{ACCm\_n}cos(nN_r\theta) - \sum_{n=2,4,6...}\psi_{ACCm\_n}cos(nN_r\theta),$$
$$m = even\ number. \tag{10}$$

where coil Cm refers to the coils that are in phase with $C1$. It is shown that the DC component and even harmonics can be completely eliminated when m is an even number. And odd harmonics can be amplified, regardless of m is an even or odd number. Taking the 24-slot and 22-rotor-tooth model presented in Fig. 1 as an example, the m value satisfying (10) is 4, 7, and 10. Thus, when coil $C1$ is connected in series with coil $C4$, $C7$, and $C10$ to form the phase A winding, the total flux is

$$\psi_{phA} = \psi_{C1} + \psi_{C4} + \psi_{C7} + \psi_{C10} = 4\sum_{n=1,3,5...}\psi_{ACC1\_n}cos(nN_r\theta) \tag{11}$$

where Ψ_{phA} is the Phase A flux when the coils are connected into winding. The DC components and even harmonics of Ψ_{C1} and Ψ_{C4} are eliminated with each other completely. And the DC components and even harmonics of Ψ_{C7} and Ψ_{C10} are eliminated with each other. Thus, only odd harmonics remain in Ψ_{phA}. It implies that the even-order harmonics in the torque can be reduced and the torque density can be effectively improved with the auxiliary flux from the slot PMs.

C. *Machine Inductance Analysis*

Similar with coil flux analysis, in this part, the machine inductance is analyzed. The self-inductance of $C11$ and $C12$ and their mutual inductance, denoted with L_{C11}, L_{C12}, and M_{C11C12}, can be expressed as

$$L_{C11} = L_{DCC11} + \sum_{n=1}^{+\infty}L_{ACC11\_n}cos(nN_r\theta) \tag{12}$$

$$L_{C12} = L_{DCC12} + \sum_{n=1}^{+\infty}L_{ACC12\_n}cos\left[nN_r\left(\theta + \frac{\pi}{N_r}\right)\right] \tag{13}$$

$$M_{C11C12} = M_{DCC11C12} + \sum_{n=1}^{+\infty}M_{ACC11C12\_n}cos(nN_r\theta) \tag{14}$$

where L_{ACC11_n}, L_{ACC12_n} and $M_{ACC11C12\_n}$ are the amplitude of the nth harmonic component. L_{DCC11}, L_{DCC12} and $M_{DCC11C12}$ are the corresponding DC components. When $C11$ and $C12$ are connected, the mutual inductance is non-negligible as $C11$ and $C12$ share the same magnetic flux path. The self-inductance of $C1$ (L_{C1}) can be expressed as

$$L_{C1} = L_{C11} + L_{C12} + 2M_{C11C12}$$
$$= L_{DCC11} + L_{DCC12} + 2M_{DCC11C12}$$
$$+ \sum_{n=1,3,5...}\left(L_{ACC11\_Mn} - L_{ACC12\_Mn} + 2M_{ACC11C12\_Mn}\right)cos(nN_r\theta)$$
$$+ \sum_{n=2,4,6....}\left(L_{ACC11\_Mn} + L_{ACC12\_Mn} + 2M_{ACC11C12\_Mn}\right)cos(nN_r\theta) \tag{15}$$

According to (15), the DC component and even harmonics are amplified, but the odd harmonics are suppressed. When coils are connected into winding, similar with (10), the self-inductance of coils in phase with $C1$ can be expressed as

$$L_{Cm} = L_{DCCm} + \sum_{n=1,3,5...}L_{ACCm\_n}cos(nN_r\theta) + \sum_{n=2,4,6...}L_{ACCm\_n}cos(nN_r\theta),$$
$$m = odd\ number. $$

$$L_{Cm} = L_{DCCm} - \sum_{n=1,3,5...}L_{ACCm\_n}cos(nN_r\theta) + \sum_{n=2,4,6...}L_{ACCm\_n}cos(nN_r\theta),$$
$$m = even\ number. \tag{16}$$

where coil Cm refers to the coils that are in phase with $C1$. It is

shown that the odd harmonics can be eliminated when m is an even number. Taking the 24-slot and 22-rotor-tooth model presented in Fig. 1 as an example, $C4$, $C7$, and $C11$ are in phase with $C1$. From the topology, it is clear that there is little flux in Cm when a constant current is applied in $C1$. Consequently, the mutual inductance among $C1$, $C4$, $C7$, and $C10$ can be neglected. Therefore, the self-inductance of phase A (L_{phA}) can be expressed as

$$L_{phA} = L_{C1} + L_{C4} + L_{C7} + L_{C10} = 4L_{DCCm} + 4\sum_{n=2,4,6...}L_{ACCm\_n}cos(nN_r\theta) \tag{17}$$

It is revealed in (17) that the odd harmonics are completely eliminated when coils are connected into winding. As is analyzed above, the even harmonics are suppressed when $C11$ is connected with $C12$, L_{phA} is very close to constant. Therefore, the proposed machine can be seen as a non-salient machine with complementary flux path, and $I_d = 0$ control can be used.

IV. MACHINE OPTIMIZATION AND PERFORMANCE ANALYSIS

A. *Machine Optimization*

In this part, the Genetic Algorithm is used to optimize the proposed machine. The optimization objectives are to maximize the rated average torque (T_{avg}) and minimize the torque ripple (T_{rip}) within the given size and current density.
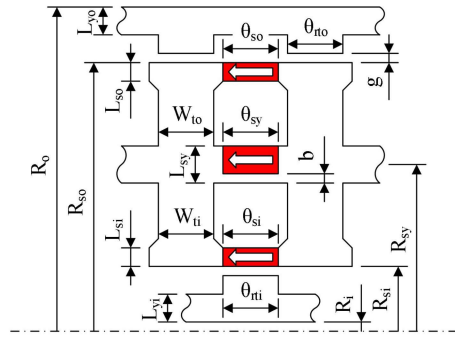

Fig. 5. Notation for dimensional parameters.

TABLE I
THE CONSTRAINS OF DESIGN PARAMETERS

Items	Notation	Value
Outer radius of outer rotor (mm)	R_o	63
Air-gap length (mm)	g	0.85
Stator core bridge thickness (mm)	b	0.5
Number of stator slots	N_{slot}	24
Number of rotor teeth	N_r	22
Estimated slot filling factor	S_{ff}	0.6
Rated current density (A/mm²)	D	5
Stack length (mm)	L_s	76

To provide a clear demonstration, the design parameters of the proposed machine are presented in Fig. 5. During the optimization, the maximum size, air gap length, current density and slot filling factor are kept constant, which are listed in Table I. The inner/outer coil turn numbers are in direct proportion to inner/outer slot areas. The optimization objectives are to maximize T_{avg} and minimize T_{rip}. Considering the tradeoff between T_{avg} and T_{rip}, the following selection standard is used to choose the optimal design:

$$k_{sel} = k_{avg}T_{avg} - k_{rip}T_{rip} \tag{18}$$

where k_{sel} is the selection standard, k_{avg} and k_{rip} is the weight of T_{avg} and T_{rip}. The model with the highest k_{sel} value is chosen as the optimal design. In this case, the values of k_{avg} and k_{rip} are set as 1 and 50, respectively. The Pareto front of each generation during the optimization is presented in Fig. 6, and the optimal design is highlighted. The corresponding design parameters are listed in Table II, where N_{out}, N_{in} and I_{ac} are referred to out coil turns, inner coil turns and armature current.

Fig. 6. Pareto front of the Genetic Algorithm.

TABLE II
THE DESIGN PARAMETERS OF OPTIMAL MODEL

Notation	Vibration Range	Optimal Value
R_i (mm)	1 - 20	13.84
L_{yi} (mm)	1 - 20	4.19
θ_{rti} (deg)	5.73 - 10.64	7.53
L_{yo} (mm)	1 - 6	3.36
θ_{rto} (deg)	5.73 - 10.64	6.22
R_{so} (mm)	52 - 58	54.9
W_{to} (mm)	1.5 - 3.5	2.52
θ_{so} (deg)	6 - 9	8.4
L_{so} (mm)	1 - 5	4.07
R_{si} (mm)	18.85 - 28.85	23.35
W_{ti} (mm)	1.5 - 3.5	2.29
θ_{si} (deg)	6 - 9	6.75
L_{si} (mm)	1 - 5	3.17
L_{sy} (mm)	3 - 10	6.22
N_{out}	Dependent	32
N_{in}	Dependent	20
I_{ac} (A)	Dependent	4.95
T_{avg} (Nm)	/	5.446
T_{rip} (Nm)	/	0.044

B. Machine Flux Distribution

In this part, the open-circuit flux distribution from yoke PMs and slot PMs are analyzed with FEA results, and the design parameters are based on the optimal model in the last part. Fig. 7 shows the flux distribution with the slot PMs and yoke PMs with frozen permeability. Taking the stator tooth marked in red as an example, the field produced by the inner slot opening PMs and yoke PMs is always outwards, while the field produced by outer slot opening PMs is always inwards. Therefore, with both inner and outer slot PM and yoke PM excitation, the DC component of flux density can mitigate and the local BH working range in the stator tooth can be extended to another quadrant. The local flux density against rotor position is presented in Fig. 8, where Ψ_{Yoke}, Ψ_{Out}, Ψ_{In}, and Ψ_{All}, represent the flux density when yoke PMs, outer slot opening PMs, inner slot opening PMs and all PMs are used, respectively. The fields produced by yoke PMs and inner slot opening PMs are positively biased, while the field produced by outer slot

opening PMs is negatively biased. When all three sets of PM excitation are used, the average value of flux density is close to zero. Therefore, in terms of local tooth saturation, the stator tooth is less saturated when all PMs are used as the maximum flux density over an electrical period is smaller than that of Ψ_{Yoke}.
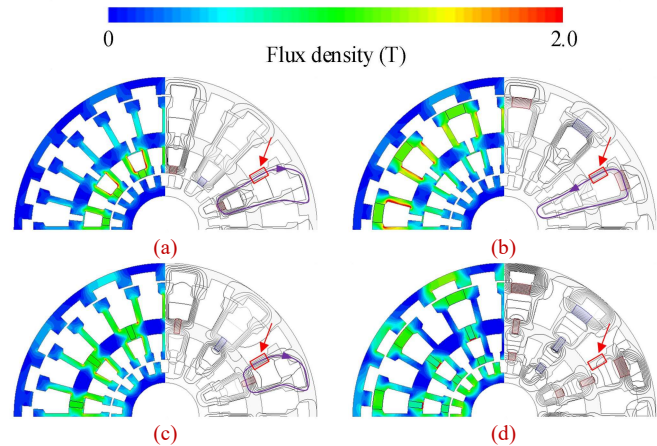

Fig. 7. Open-circuit flux distribution. (a) With only inner slot PMs. (b) With only outer slot PMs. (c) With only yoke PMs. (d) With all PMs.
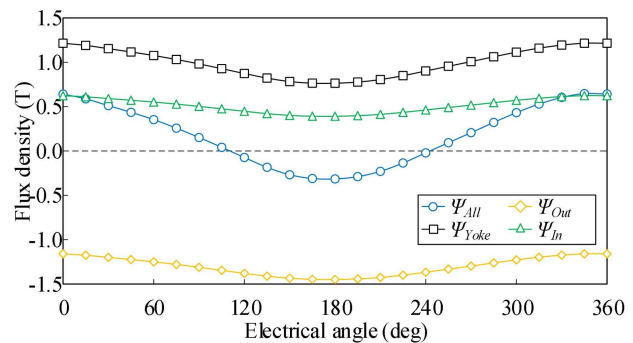

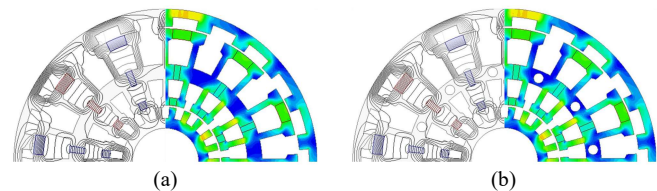Fig. 8. Open-circuit flux density in the stator tooth.

Fig. 9. Flux distribution under load condition. (a) Without nails on the stator. (b) With nails on the stator.

The flux distribution under load condition is presented in Fig. 9(a). The machine is less saturated because of the improved stator core utilization factor by slot opening PMs. In Fig. 9(b), some nails are used to fix the stator with the shell, and it can be found that there are little changes in flux distribution because the nails are not located at the main flux path. The radial magnetic force is close to zero because of the slot/pole combination of 24/22 and associated symmetrical flux.

The open-circuit flux and corresponding harmonics obtained by Fast Fourier Transform are presented in Fig. 10 and Fig. 11. Taking coil $C11$ as an example, as is shown in Fig. 10, although Ψ_{C12_M} is positively biased, the DC component of Ψ_{C12} is almost equal to zero, namely not biased thanks to the introduction of additional slot PMs. Therefore, it validates that the BH working

range of the stator core can be extended to another quadrant.

In Fig. 11, when four coils are connected into winding, the DC and even harmonics of Ψ_{phA} are completely eliminated under complementary rotor structure. Ψ_{phA} has a nearly perfect sinusoidal waveform, in spite of a little 3rd harmonics, which can be eliminated with Y connected winding configuration. Actually, Ψ_{C1}, Ψ_{C4}, $\Psi_{C7,}$ and Ψ_{C10} are also very sinusoidal thanks to the optimization algorithm because torque ripple is set as one of the optimization objectives.

Fig. 10. The open-circuit flux of $C11$. (a) Waveform. (b) Harmonics.

Fig. 11. Open-circuit flux linkage in A phase. (a) Waveform. (b) Harmonics.

C. Torque contribution analysis

In the proposed design, using frozen permeability, the torque contributions of yoke PM, outer PM and inner PM are 1.74 Nm (31.8%), 2.37 Nm (43.6%) and 1.34 Nm (24.6%), respectively.

To reveal the influence of the balance between the two rotors, the ratio of circumferential diameters of two airgap lines is analyzed, which is defined as

$$k_{ad} = \frac{D_{in}}{D_{out}} \tag{18}$$

where D_{out} and D_{in} are the circumferential diameters of the outer airgap line and inner airgap line, respectively. And k_{ad} is the ratio of circumferential diameters of two airgap lines. The torque production against different k_{ad} is presented in Fig. 12, where T_{Out}, T_{In} and T_{Total} are outer rotor torque, inner rotor torque and total torque, respectively. All the dimensional parameters are selected from the optimization result of the Genetic Algorithm except for k_{ad}. The value of k_{ad} in optimal design is marked in Fig. 12, which varies from 0.29 to 0.49.

When higher k_{ad} value is used, the diameter of inner rotor is relatively higher. Therefore, the torque production of inner rotor can be promoted. However, higher k_{ad} value brings relatively smaller stator slot area, which leads to smaller current as the current density is kept constant. Therefore, the torque production of the outer rotor is suppressed at high k_{ad} region. Considering the tradeoff between torque productions of two rotors, the optimal value for k_{ad} lies on roughly 0.41 in this case.
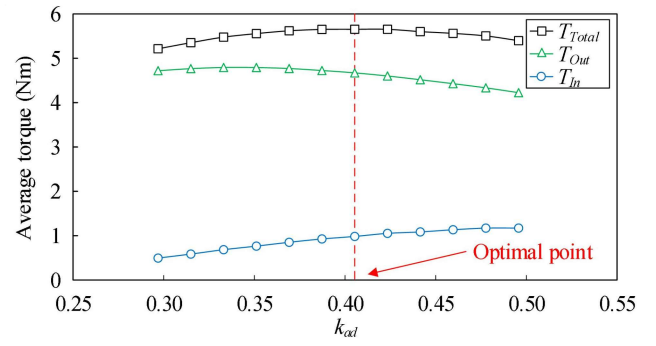

Fig. 12. Torque contribution of two rotors and total torque production under different k_{ad}.
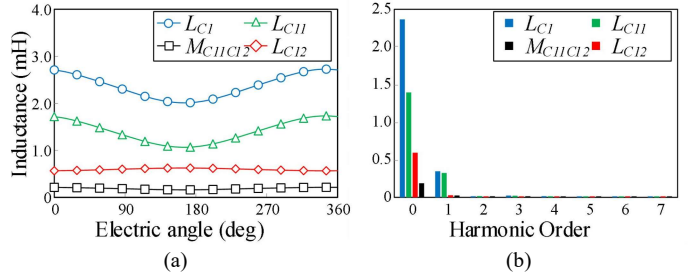
D. Machine Inductance

Fig. 13. Self and mutual inductance of coils. (a) Waveform. (b) Harmonics.
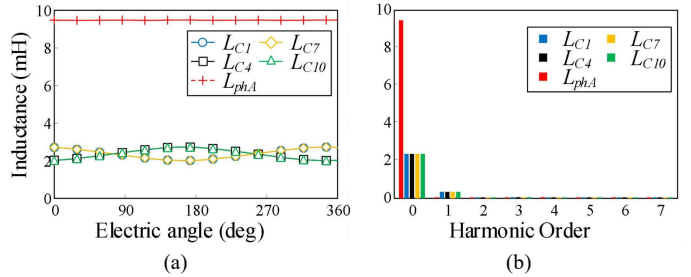

Fig. 14. The inductance of winding and coils. (a) Waveform. (b) Harmonics.

The self-inductance and mutual inductance of $C11$ and $C12$ are presented with the self-inductance of $C1$ in Fig. 13. As is analyzed in (15), the odd harmonics of L_{C11} and L_{C12} mitigate each other. Therefore, the fundamental harmonics of L_{C11} and L_{C12} have opposite polarity, although their amplitudes are different. For even harmonics, the even harmonics of L_{C1} are also very low, although they are amplified when $C11$ is connected with $C12$ because the even harmonics of L_{C11} and L_{C12} are very low in this case.

The winding self-inductance (Phase A) is presented with L_{C1}, L_{C4}, L_{C7} and L_{C10} in Fig. 14. As is analyzed in (17), even harmonics are completely eliminated. L_{phA} is a nearly perfect constant, and therefore the proposed machine can be seen as a non-salient machine with complementary flux path, and $I_d = 0$ control can be used.

E. Machine Comparative Study

To show the validity of complementary rotor structure and additional slot PMs, the machines with/without slot PMs and complementary rotor structure are analyzed. Based on the optimal design in the previous part, the performances of three machines are presented, where Machine I is the proposed machine, Machine II has a complementary rotor but no slot PM,

Machine III has slot PM but the angle shift between two rotors is 0, rather than 180 deg (shown in Fig. 15).
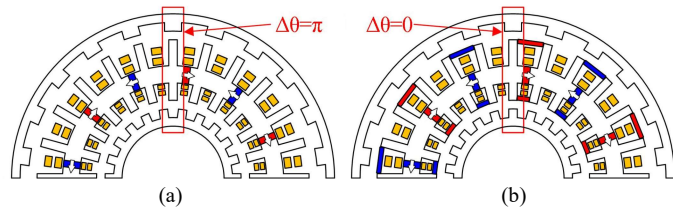

Fig. 15. Machines for comparison with the proposed machine. (a) Machine II without slot PMs. (b) Machine III without complementary structure.

The back EMF and the associated harmonics obtained by Fast Fourier Transform are presented in Fig. 16 at speed of 600 rpm. The THDs of them Machine I, II, and III are 8.92%, 9.02%, and 11.70% respectively. The machine I has the highest back EMF and lowest THD among the three models.

Fig. 16. Open-circuit back EMF. (a) Waveform. (b) Harmonics.

Fig. 17. Torque production.

Fig. 17 shows the rated torque production of three machines, where $I_d=0$ control is used. All machines can produce smooth torque. The torque ripple ratios of Machine I, II and III are 0.81%, 1.13% and 1.61%, respectively. The proposed machine has the highest torque production and lowest torque ripple ratio, which proves that the proposed machine has good reliability in terms of vibration caused by torque ripple.
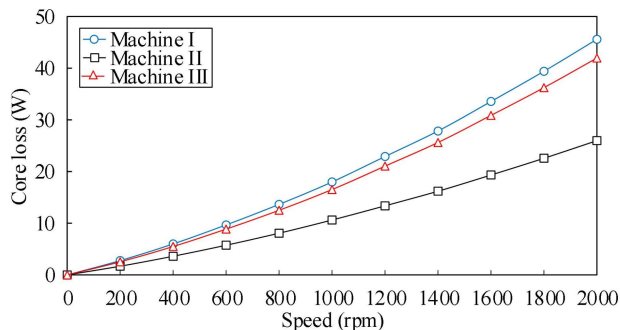

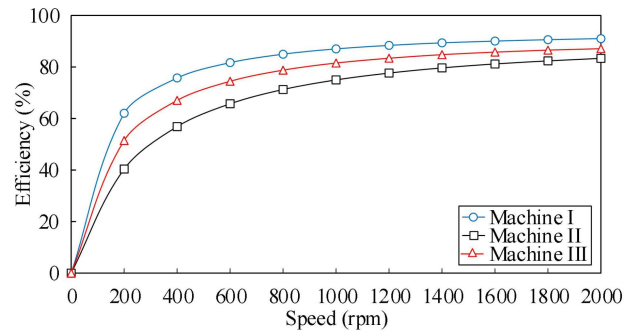Fig. 18. Core loss under different speed.

Fig. 19. Efficiency under different speed.

The dual-rotor structure has more bearings than the traditional single-rotor structure. There are two air gaps, which bring higher frictional torque and associated mechanical loss. However, the frictional torque is very small compared with electromagnetic torque. Therefore, it is still acceptable to use a dual-rotor structure considering the superiority resulting from complementary rotor structure.

In terms of copper loss, three machines have the same copper loss as they have the same stator dimensional parameters. The copper loss of three machines under rated current is 66.97W. Fig. 18 and Fig. 19 show the core loss and efficiency of the three models under rated current. The copper loss can be seen as a constant number if the skin effect is neglected, which is larger than the core loss in the three models. In the high-speed region, in spite of the growth of core loss, higher efficiency can be achieved as electromagnetic torque is in direct proportion to rotation speed. The growth of efficiency as speed is very slow when speed exceeds roughly 1000 rpm. The proposed machine can achieve the highest efficiency despite the highest core loss.

V. EXPERIMENTAL VALIDATION

To verify the above-mentioned analysis, a prototype of the proposed machine was manufactured, which is presented in Fig. 20. The design parameters are based on the optimal model from the genetic algorithm. The experiment setup is presented in Fig. 21. As is analyzed above, the proposed machine can be regarded as a non-salient machine, because of complementary flux path. The conventional $I_d=0$ vector control for synchronous machines can be applied to the proposed machine directly.

The measured open-circuit back EMF of the prototype is presented in Fig. 22, together with the FEA simulated results at the rotation speed of 600 rpm. The data shows that the experimental result agrees with the FEA result well.

The torque-current angle curve is also measured and displayed together with the simulated result in Fig. 23, where the armature current is set at the rated value. It can be found that the curve is very sinusoidal, which agrees with the above analysis on winding inductance well. When $I_d=0$ control is used, the torque production under different currents is presented in Fig. 24. The frictional torque is roughly 0.14 Nm at the rated condition, which is only 2.5% of the rated electromagnetic torque (5.45 Nm). Based on the measured torque and simulated core loss, the efficiency at 600 rpm of the prototype can be calculated and presented in Fig. 25, which agrees with FEA results well.
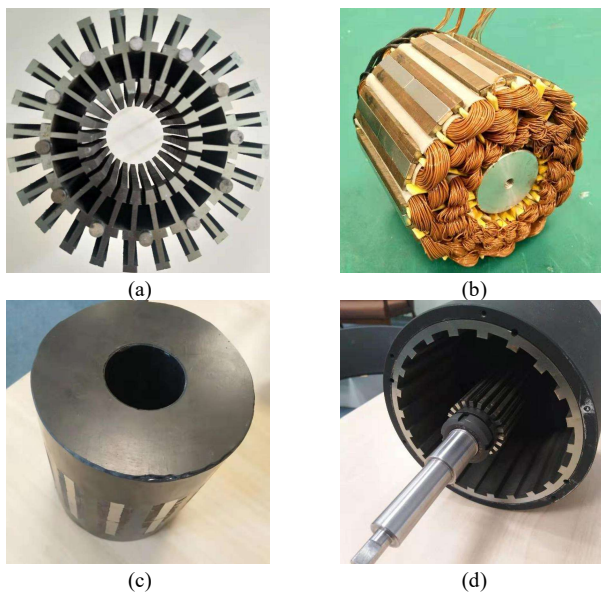
Fig. 20. The picture of the prototype. (a) Stator core. (b) Stator with winding. (c) Stator with epikote. (d) Complementary rotors with mechanical connection.
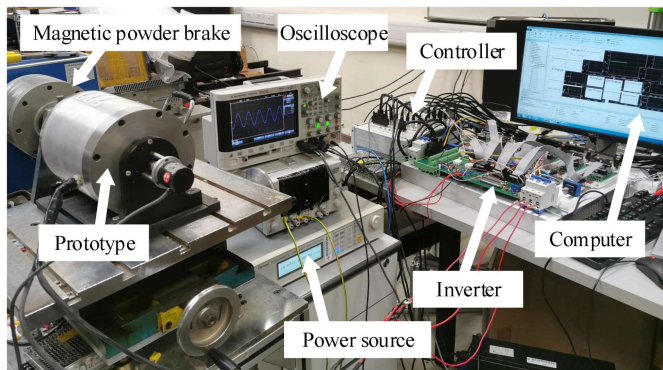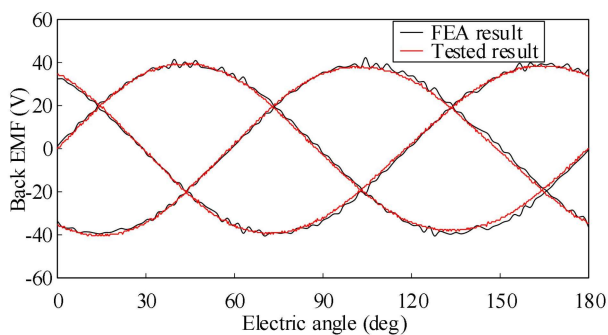

Fig. 21. Experiment setup.

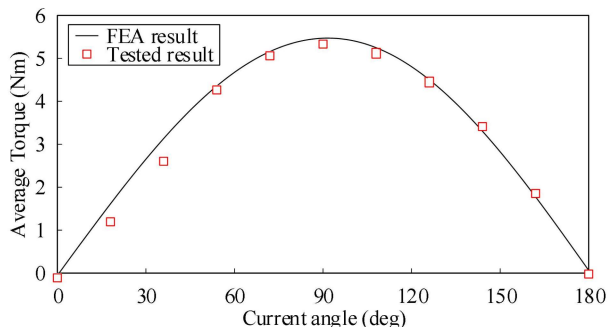Fig. 22. Tested open-circuit back EMF and FEA result.

Fig. 23. Tested output torque and simulated electromagnetic torque.
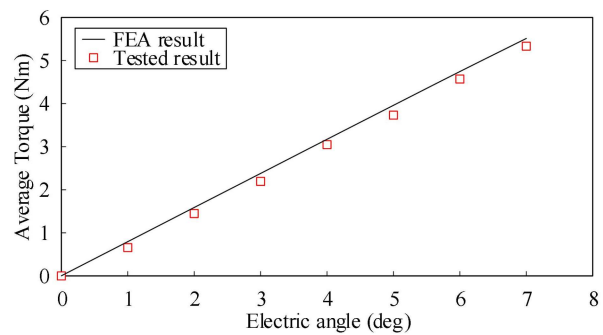

Fig. 24. Measured rated output torque and FEA electromagnetic torque under different currents.
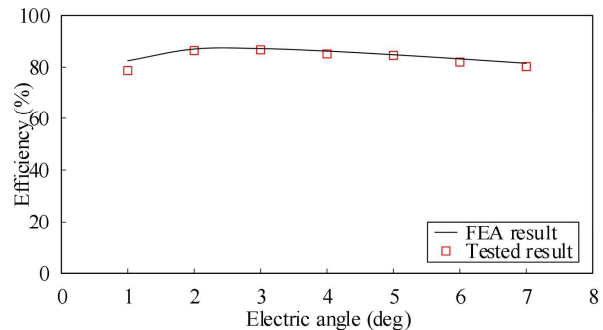

Fig. 25. Tested efficiency and FEA value under different current.

VI. CONCLUSION

This paper proposes a novel DSPMM with three groups of parallel-excited PMs. And the complementary rotor structure provides a commutative flux path for PMs so that the PM flux can avoid being opened, and leakage flux and resultant cogging torque can be suppressed. It is revealed in the stator core flux analysis that the DC component and even order harmonic of coil flux can be eliminated and therefore the good sinusoidal back EMF and smooth torque can be obtained. The main field is built by the yoke PM, which has higher PM utilization because the yoke PM flux switches between two rotors without been shorted. The auxiliary field is built by the slot PM, which promotes the stator core utilization factor because the BH working range of the stator can be extended to another quadrant. Thus, some trade-offs must be considered between yoke PMs and slot PMs. In this paper, the genetic algorithm is used to find optimal design parameters of the proposed machine. Based on the optimization result, a comprehensive comparison among the proposed machine and the other DSPM machines is carried out. It is shown that the proposed machine has the highest torque production, highest efficiency, lowest torque ripple and lowest THD of back EMF, which validates the superiority of the additional slot PMs and complementary flux path. In the proposed machine, when both yoke PMs and slot opening PMs are used, the average torque is 1.45 times higher than that of the machine without slot opening PMs. Besides, the torque ripple is reduced from 1.61% to 0.81% when complementary rotor structure is used. A prototype is tested and the results agree with FEA results well.